

Prediction of the Gas Emission from Porous Media with the concern of Energy and Environment

Ahmed Al Makky.¹, A.Alaswad², Desmond.Gibson³ and A.G.Olabi⁴

1. School of Engineering, University of the West of Scotland, Paisley; email: Ahmed.AIMakky@uws.ac.uk
2. School of Engineering, University of the West of Scotland, Paisley; email: Abed.Alaswad@dew.ac.uk
3. Scottish Universities Physics Alliance, Institute of Thin Films, Sensors & Imaging; Des.Gibson@uws.ac.uk
4. School of Engineering, University of the West of Scotland, Paisley; email: Abdul.Olabi@uws.ac.uk

Abstract

Measuring soil carbon dioxide efflux is a challenging task even when it is performed using respiration chambers. While gas samples are taken, measurement deviations become more evident according to the used chamber design especially when external disturbances occur.

This paper studies the carbon dioxide concentration profiles within the top soil layers, and investigates the controlling factors affecting the process. The considered factors are diffusion, temperature and viscosity. The efflux equation is discussed and then it is linked with the soils geotechnical parameters, while a relationship between the Reynolds number within the soil and efflux is found. Emphasis on the importance of the external geometrical design considerations is shown through studying external boundary layer effects due to the chamber outer shell shape and how it interacts with blowing winds. Chamber stability on site of deployment is also of a significant importance considering external blowing winds. Internal geometrical considerations are linked with the flow turbulence within the dynamic chambers. It is highly recommended that respiration chamber designers need to work in parallel with a multidisciplinary team in order to make a chamber design that ensures the least disturbance to occur at the location of study.

Keywords: CO₂, Soil Porosity, Permeability, Dynamic Chambers, Global Warming, Renewable Energy,

- Abbreviations

CFD

PDE

IPCC

EAHE

Computational Fluid Dynamics

Partial Differential Equation

Intergovernmental Panel on Climate Change

Air Heat Exchanger System

- Roman Symbols

A	Sample area cross section
---	---------------------------

1	A_s	Covered soil surface area by chamber
2	A_f	Flow obstructing chamber area
3	C_D	Drag force coefficient
4	D_{Fan}	Blowing fan diameter length
5	D_{CO_2}	The gas diffusion coefficient for carbon dioxide
6		
7	D_e	Effective gas diffusion coefficient
8		
9	$D_{(CO_2)_0}$	Diffusion coefficient at reference state
10	\bar{d}	Average characteristic length scale for pores
11	ef	efflux
12	ef_{soil}	Gas efflux for a soil layer
13	$ef_{chamber}$	Gas efflux
14	ef_{total}	Carbon dioxide total efflux
15	ef_{Plants}	Carbon dioxide efflux from plants
16	$ef_{Bacteria}$	Carbon dioxide efflux from bacteria
17	Ef_{total}	None-dimensional form of the efflux
18	$ef_{tDynamic}$	Dynamic total efflux measurement
19	ef_{tStaic}	Total static efflux
20	$ef_{Location}$	Respiration quotients for different soil locations
21		
22	F_{wind}	Acting wind force
23	F_w	weight force
24	f	vortex shedding frequency
25	g	Gravitational acceleration
26	H	Chamber height
27	h	Lever arm for the wind force
28	Y_{CO_2}	Gas species concentration
29	k	Soil sample permeability
30	L	Soil layer depth thickness
31	L_s	Characteristic dimension
32	MW_{CO_2}	Carbon dioxide molecular weight
33	P	Pressure
34	P_0	Reference pressure
35	P_{TS}	Total top soil pressure (surface)
36	P_{TB}	Total bottom soil pressure
37	$P_{SurfaceCO_2}$	Carbon dioxide partial pressure at soil surface
38	$p_{BottomCO_2}$	Carbon dioxide partial pressure at soil bottom of soil layer
39	Re_s	Reynolds number for soil (porous media)
40	$RQ_{Location}$	Respiration quotient for a specific location
41	RQ_{GL}	Respiration quotient for grassland
42	$RQ_{Location}$	Respiration quotients for different soil locations
43		
44	Q_{CO_2}	Carbon dioxide volumetric flow rate
45	q_{CO_2}	Darcean velocity
46	Re	Boundary layer Reynolds number
47		
48		
49		
50		
51		
52		
53		
54		
55		
56		
57		
58		
59		
60		
61		
62		
63		
64		
65		

Re_{cr}	Critical Reynolds number
Re_x	Boundary layer Reynolds number at distance x
St	Strouhal Number
T_0	Reference temperature
u_∞	free stream velocity
\bar{U}	Average flow velocity at the studied location
u_{cr}	Critical blowing wind velocity
V_c	Chamber volume
V_e	Effective chamber volume
V_c	volume of the chamber
v_{CO_2}	Average pore velocity for carbon dioxide
T_n	Summation of all torque components
T_{wind}	Wind torque
T_{weight}	Weight torque
x	The distance downstream from the start of the boundary layer
z	Function of elevation
z_{gs}	Distance from the soil surface to the tip of the gas sensor
$[CO_2]$	Concentration of carbon dioxide
$[O_2]$	Concentration of oxygen
$[CO_2]_s$	Molar concentration of carbon dioxide on the soil surface
$[CO_2]_B$	Molar concentration of carbon dioxide at the bottom of the soil surface

- Greek Symbols

α_s	Carbon dioxide source term starting from the soil surface
α_{gs}	Carbon dioxide source term starting from the soil depth
δ	Soil constructivity
δ	Boundary layer thickness
τ	Soil tortisity
ν	kinematic viscosity
ε	Average rate of dissipation per unit mass
η	Kolmogorov length scale
μ	Air dynamic viscosity
μ_{CO_2}	Carbon dioxide gas viscosity
ρ	Air density
ρ_{CO_2}	Carbon dioxide density
∇p_{CO_2}	Carbon dioxide pressure gradient

1.1 Introduction

The research work towards developing sustainable and clean energy is advancing through the last four decades as fossil fuels which are widely used as the main energy resources are not sustainable, and significantly linked to the climate change issue. Climate change is increasingly becoming one of the most serious global challenges due to the rapid increase of the greenhouse gases (mainly CO₂, CH₄ and N₂O) in the atmosphere [1, 2]. In order to understand the rate of greenhouse gases accumulation and to measure or compare different control proposals, it is very important to measure accurately the greenhouse fluxes between the soil and the atmosphere [3, 4]. Soil can be defined as a complex system, consisting of a mixture of organic and mineral particles, soil solution and air, resulting from the interaction between biotic and abiotic factors; it is the medium in which plants acquire water and nutrients through their roots system [5]. This results in a carbon dioxide efflux that flows out and forth from the biologically active soil layers. Due to that the total carbon dioxide efflux is a summation of many sub effluxes. Measuring accurately the production of gas species from the soil is not easy. Spatial variability in soil emissions and the quantification of these emissions is complicated by the high spatial variability exhibited by many microbial processes [6]. This spatial variability is enforced by the soil chemical composition which varies significantly from one location to another [7]. Respiration chambers are used to measure carbon dioxide efflux of location this is through accumulating the gas mixture in an enclosed gas volume within the chamber. Henrik Lundegardh [8] was the first to propose the concept in the form of the respiration bell. Site fertility assessment is the objective whereby carbon dioxide rate of production is the indicator. This means the different soil locations contribute differently to global warming due to difference of site fertility [9]. Consequently with the increase of carbon dioxide concentrations in the atmosphere, planet earth responds to it in the form of the green house affect [10]. This has lead scientists to use numerical

1 nonlinear models to predict future concentrations of carbon dioxide in the atmosphere [11],
2 on the other hand others used more sophisticated models like the dynamic global vegetation
3 model [12] as shown in Figure 1.
4
5
6
7
8
9

10
11 **Figure 1:** IPCC IS92a projections of atmospheric CO₂ concentration and the HadCM2 SUL
12 climate model simulations of temperature over land (excluding Antarctica).
13 For instance global warming is attributed to burning excessive amounts of fossil fuels [13].
14
15
16 The drive is always to reduce carbon dioxide emissions by lessening the industrial source of
17 the gas. Lessening the production of the carbon dioxide gas requires the reliance on a clean
18 energy source such as wind power as stated by Evans et al [14]. Human rise of population
19 also contributes in the increase of energy consumption. Therefore using sustainable sources
20 of energy that don't produces carbon dioxide to support the growing demand for energy
21 comes of priority, this if for the case of strategic future planning by governments, as the study
22 by Omer [15] showed for the country of Sudan. Computational hardware and optimization
23 algorithms are developing rapidly. Hence computer software can assist governments in
24 making future plans and predictions to expected energy demands. This is to manage
25 renewable energy sources according to its availability characteristics as shown by Banos et al
26 [16].
27
28
29
30
31
32
33
34
35
36
37
38
39
40
41
42
43

44 In most African countries forest resources are gradually declining. Hence the supply of fuel
45 wood is becoming more difficult to sustain and demand. Especially that it is already
46 exceeding the potential supply as shown by Bugaje [17]. Therefore governments need to
47 apply policies that make citizens gradually use less fossil fuels [18]. New sustainable source
48 of fuels are being introduced to the global market like the Malaysia palm oil example which
49 is considered one of the most productive bio-diesel crop. Its waste streams can be used to
50 produce vast amounts of bio-gas and other values added products [19]. Another sustainable
51
52
53
54
55
56
57
58
59
60
61
62
63
64
65

1 type of fuel is ethanol which still requires more research to prove its environmental
2 friendliness. This is shown by Niven [20] in his comparison between E10 and E0. Microalgae
3
4 is another attractive biodiesel fuel that can be considered as a substitute fuel. It is still in the
5
6 phase of development [21] and the issue of the reduction of its production cost is still posing
7
8 as a challenge.
9

10
11
12 A way to assess renewable sources of energy is to apply exergetic analysis on them as shown
13
14 by Hepbasli in [22]. Life cycle assessment for renewable source of energy is also necessary as
15
16 stated by Bhat and Prakash [23] for electrical generation systems. Alanne and Saari noted in
17
18 [24] that energy systems of the future are going to be a mixture of centralized and distributed
19
20 sub-systems, operating parallel to each other.
21
22
23
24

25
26 In this paper: several efflux models are covered focusing mainly on the physical and geo-
27
28 mechanical side of the species transport process in the soil with the proposal for the use of a
29
30 relationship linking efflux with the respiration quotient of a location. A link between efflux
31
32 and inner soil gas species flow velocity is found through the efflux Reynolds number
33
34 equation. Furthermore respiration chamber shape and operational mode is covered whereby
35
36 both are linked with chamber design regulations. For chamber design operational
37
38 enhancement inner and outer geometrical factors are covered. Likewise the interaction of the
39
40 chamber outer shell with local boundary layer produced by locally blown winds is discussed.
41
42
43 This is for the three used common shapes of cylindrical, box and hemispherical. Lastly a
44
45 chamber static stability formula is derived for different shapes to assist designer to predict
46
47 which wind speeds cause chamber tip over.
48
49
50
51
52

53 **1.2 Soil Carbon dioxide efflux Model**

54
55
56 Through the discussion of simple analytical models to calculate carbon dioxide flux in
57
58 reference [25] stated that 75% of the efflux comes from the top 20 cm of the soil. This means
59
60
61

1 that the atmospheric soil interface is the place to start building the numerical model. Any site
2 location has a set of standard soil layers that have been characterized by geotechnical
3 engineers.
4
5

6 7 8 **1.2.1 Chamber Gas Volume efflux** 9

10 By considering the most biologically activate ones near the top soil surface can help in
11 modelling the produced efflux. Assuming no external disturbances occur and by applying
12 Fick`s first law in in the z direction. The considered ideal efflux is the static efflux, which
13 represents a steady case where the species concentration profile does not change with time.
14 Applying Fick`s first law on the gas part of the chamber results in equation (1.1). Where
15 ef_{chamber} is the gas flux [$\mu\text{mol m}^{-2}\text{s}^{-1}$]. The term D_{CO_2} is the gas diffusion coefficient for
16 carbon dioxide in the contained air in the chamber [m^2s^{-1}]. Gas diffusion is a function of
17 temperature, once the chamber average temperature is obtained gas diffusion can be found
18 from [26].
19
20
21
22
23
24
25
26
27
28
29
30
31
32

$$33 \quad ef_{\text{chamber}} = -D_{\text{CO}_2} \frac{\partial Y_{\text{CO}_2}}{\partial z} \quad (1.1)$$

34
35
36
37 Trace gas species concentration Y_{CO_2} [$\mu\text{mol m}^{-3}$] is a function of elevation z [m] inside the
38 chamber and can be represented by equation (1.2), the distance z_{gs} [m] is from the soil
39 surface to the tip of the gas sensor. The carbon dioxide source term starting from the soil
40 surface is α_s [$\mu\text{mol m}^{-3}\text{s}^{-1}$], this term incorporates soil bacterial, plant root, and plant leaf
41 activity.
42
43
44
45
46
47
48
49
50

$$51 \quad Y_{\text{CO}_2} = \frac{\alpha_s}{2D_{\text{CO}_2}} (z_{\text{gs}}^2 - z^2) \quad (1.2)$$

1.2.2 Soil Volume efflux

Fick's first law can also be applied to the soil part entrained under the chamber [27] as shown in equation (1.3) for simplicity it can be applied for one standard soil layer. The gas efflux for a soil layer is ef_{soil} [$\mu\text{mol m}^{-2}\text{s}^{-1}$]. The effective gas diffusion coefficient D_e [m^2s^{-1}] as proposed by [28] for carbon dioxide in the air in the soil pores. The trace gas concentration Y_{CO_2} [$\mu\text{mol m}^{-3}$] is a function of the vertical position z (m) in the soil:

$$ef_{\text{soil}} = -D_e \frac{\partial Y_{\text{CO}_2}}{\partial z} \quad (1.3)$$

The controlling parameters of D_e are presented in equation (1.4) where ϕ is the air porosity in the soil location. The term δ is soil constructivity which usually takes a value of 0.9 to 1, it depends on how compact are the fine soil particles are at the location. Soil tortuosity is represented by τ and takes values from 0.5 to 6 as shown in [26] it all depends on the effective pore diameters created by rocks in the soil layer:

$$D_e = \frac{\tau D_{\text{CO}_2} \phi}{\delta} \quad (1.4)$$

Equation (1.3) can be extended to consider several layers of soil. During the sampling duration of an experiment heat affects the diffusion process in both the chamber gas entrainment and the covered soil by the chamber. The diffusion coefficient for two states can be found relying on [26], looking at equation (1.5) the diffusion coefficient for carbon dioxide at the studied state is D_{CO_2} [m^2/s] while for the reference state is $D_{(\text{CO}_2)_0}$ [m^2/s]. The reference temperature is T_0 [K] while the reference pressure P_0 [Pa]. Likewise the studied case temperature is T [K] while the studied state pressure is P [Pa]. As evident the diffusion coefficient for carbon dioxide is proportionally related to the temperature term $T^{3/2}$ while it is disproportionally connected with the pressure term P [Pa]. Soil either gains heat or losses

1 it depends on the daily cyclic heat pattern, diffusion in soil cavities is enhanced by
 2 temperature rise as shown in the following equation:
 3
 4

$$5 \quad D_{CO_2} = D_{(CO_2)_0} \left(\frac{T}{T_0} \right)^{3/2} \frac{P_0}{P} \quad (1.5)$$

6
 7
 8
 9
 10 Equation (1.5) proves that the diffusion coefficient in soil cavities is proportionally related to
 11 small pressure changes, hence low pressure atmospheric disturbances contribute to measured
 12 efflux deviations. It also proves the temperature sensors need to be used at locations inside
 13 the soil layer. By substituting equations (1.3) and (1.4) into the Reynolds transport equation
 14 the relation of concentration and soil depth can be found in equation (1.6). The trace gas
 15 concentration in the soil is Y_{CO_2} [$\mu\text{mol m}^{-3}$] and z_d [m] is the vertical position from the soil
 16 depth to the soil surface. The carbon dioxide source term starting from the soil depth is
 17 α_{gs} [$\mu\text{mol m}^{-3}\text{s}^{-1}$], this term can incorporate soil bacterial and plant root activity.
 18
 19
 20
 21
 22
 23
 24
 25
 26
 27
 28
 29
 30

$$31 \quad Y_{CO_2} = \frac{\alpha_{gs}\delta}{2\tau D_{CO_2}\phi} (z_d^2 - z^2) \quad (1.6)$$

32
 33
 34
 35
 36 In conclusion static chambers rely mainly on diffusion for mass transport which is a
 37 kinematic property as seen in equations (1.1) and (1.3). Both equations are used for a steady
 38 state case where the efflux does not change with time, which is by taking two concentration
 39 measurements at the start and end of the soil layer. Equation (1.3) is used in the soil gradient
 40 method. Equations (1.2) and (1.5) main advantage is they can easily model the concentration
 41 profile inside the chamber and in a soil layer as a function of elevation. Consequently by
 42 curve fitting the experimental data the volumetric source term α_{gs} in equation (1.6) can be
 43 found. Experimentally this link between the soil and chamber entrainment efflux has been
 44 verified by [29] showing a relationship between efflux and soil parameters covered in
 45 equation (1.6). That was by capturing the carbon dioxide concentration plots in relation to
 46
 47
 48
 49
 50
 51
 52
 53
 54
 55
 56
 57
 58
 59
 60
 61
 62
 63
 64
 65

1 soil depth inside the chamber and soil. Some researchers [30] proposed in order to get
 2 accurate efflux measurements is to decompose the carbon dioxide total efflux ef_{total} into
 3
 4 different flux components relating to the different sources of it in the soil as shown in
 5
 6 equation (1.7), relating to sources ranging between plant, root and microbial fluxes.
 7

$$10 \quad ef_{total} = \sum_1^N ef_n = ef_{Bacteria} + ef_{Plants} + \dots + ef_N \quad (1.7)$$

11
 12
 13
 14
 15
 16 For a conducted experiment when data analysis comes in place some researchers have used
 17
 18 the none-dimensional form of the efflux Ef_{total} when using dynamic chambers, this is shown
 19
 20 in equation (1.8). The dynamic total efflux measurement $ef_{tDynamic}$ is normalized by the total
 21
 22 static efflux ef_{tStaic} .
 23
 24

$$25 \quad Ef_{total} = \frac{ef_{tDynamic}}{ef_{tStaic}} \quad (1.8)$$

26
 27
 28
 29
 30
 31
 32 Experimentalists in [31] and many others use equation (1.9), it can be derived from the
 33
 34 Reynolds transport equation. It represents the case of rise of carbon dioxide concentration in
 35
 36 relation to time in a respiration chamber from ambient concentration to the state of species
 37
 38 saturation. The state of species saturation in the chamber is identified when any discrete
 39
 40 increase in concentration doesn't change the efflux slope. The power of this model is that it
 41
 42 can be applied to an unsteady case for both a closed static or dynamic chamber.
 43
 44 Concentration is measured in relation to time this is represented by the derivative $\partial Y_{CO_2} / \partial t$
 45
 46 [mole/m³s] with time. While V_c [m³] is chamber volume and A_s [m²] covered soil surface
 47
 48 area by chamber:
 49
 50
 51
 52

$$53 \quad ef = \frac{V_c}{A_s} \frac{\partial Y_{CO_2}}{\partial t} \quad (1.9)$$

1 A linear regression model is applied to curve fit the experimental data where equation (1.9)
 2 can also be extrapolated. Its simplicity comes from that it constitutes to several process
 3 (biological, mass convective and diffusive) occurring inside the chamber and location soil.
 4 Things become more complex for an unsteady case inside the chamber when species
 5 diffusion and convection are considered in the model as shown in equation (1.10):
 6
 7
 8
 9
 10

$$\begin{aligned}
 & \frac{\partial \rho Y_{CO_2}}{\partial t} + \rho \left(u \frac{\partial Y_{CO_2}}{\partial x} + v \frac{\partial Y_{CO_2}}{\partial y} + w \frac{\partial Y_{CO_2}}{\partial z} \right) & (1.10) \\
 & = D \left(\frac{\partial^2 Y_{CO_2}}{\partial x^2} + \frac{\partial^2 Y_{CO_2}}{\partial y^2} + \frac{\partial^2 Y_{CO_2}}{\partial z^2} \right) + \alpha_s
 \end{aligned}$$

11
 12
 13
 14
 15
 16
 17
 18
 19
 20
 21
 22 Equation (1.10) is not feasible to be solved by hand. It is solved using numerical methods for
 23 PDEs, solving it by hand is very tedious and time consuming. Hence this requires the use of
 24 computational fluid dynamics software.
 25
 26
 27
 28
 29

30 **1.2.3 Soil efflux Relating to RQ**

31
 32 One way for developing efflux models is to consider grass land physical and geo-mechanic
 33 properties to build the model. A grass land is regarded by the scientific community as an
 34 ideal case for optimum biological activity [32], besides the idea that vast areas of planet earth
 35 are covered by grass [33]. By measuring the carbon dioxide production, atmospheric oxygen
 36 consumption can be measured for a certain location. The consumption of oxygen all depends
 37 on the studied site soil structure, meaning that aeration is important for the production of
 38 carbon dioxide. The respiration quotient [34] in equation (1.11) is defined as the ratio of
 39 [CO₂] Produced [mol/m³s] over [O₂] Consumed [mol/m³s] for a pre-defined volume of
 40 soil:
 41
 42
 43
 44
 45
 46
 47
 48
 49
 50
 51
 52
 53
 54
 55
 56
 57
 58
 59
 60
 61
 62
 63
 64
 65

$$RQ_{Location} = \frac{[CO_2]}{[O_2]} \quad (1.11)$$

1 The Respiration quotient for a specific location such as a grassland land [35] is $RQ_{GL} =$
2 1.3 $[\text{mol CO}_2 \text{ mol}^{-1} \text{ O}_2]$. Researchers have already found the respiration quotients for
3 different soil locations (grassland, peatland, forest site, rangeland, etc.). Hence site location
4 oxygen consumption can directly be found instantaneously when the carbon dioxide efflux is
5 measured. Proving that each location has its characteristic efflux is based on substituting
6 equation (1.11) into (1.9) which gives equation (1.12)

$$ef_{\text{Location}} = \frac{V_c}{A_s} [\text{O}_2] RQ_{\text{Location}} \quad (1.12)$$

21 **1.3 Soil Parameters that affect CO2 efflux**

22 The soil carbon dioxide efflux challenge can be summarized into the four research lines
23 mentioned in [8]: soil chemistry, physical mechanism, physiological research line and the
24 ecological research line. The soil chemistry research line will be covered on page **Error!**
25 **Bookmark not defined..** Likewise the ecological research line will focus on resilience
26 ecology. The physiological research line that focuses on the environmental interactions with
27 soil as mentioned by authors [36, 37] which have connected soil efflux to soil biology and
28 physics. Bulk density is an indicator of soil compaction and soil health as found by authors in
29 [38]. Carbon dioxide is produced by the living organisms in the soil at different scales [39],
30 organisms activity is governed mainly by temperature, minerals, air and water content. Any
31 of these factors if not provided in a substantial quantity has an impact on the metabolism
32 process. Mainly the focus here in this section is the physical mechanism. The recommended
33 approach to study the physical mechanism is very much like the one adopted by [40] for a
34 dynamic chamber case. Where an artificial experiment is built that has all the soil parameters
35 that affect the efflux, then exploring the direct and indirect effects of them by changing their
36 values to see what soil efflux changes occurs. What is realised from the paper in simple
37 context, excluding external disturbances such as atmospheric temperature and pressure,

1 carbon dioxide fluxes are governed mainly by the constraints of soil structure. Another
2 approach taken by [41] is to apply a sensitivity analysis case to the soil parameters of interest,
3
4 where by fixing several parameters and changing one in reasonable ranges can give good
5 results for efflux predictions.
6
7

8
9
10 In conclusion from the previous discussion and supporting the physical mechanism research
11 line. It seems to be evident that what controls the carbon dioxide mass transport process is the
12 soil cavities as mentioned by [42, 43] which are indicated explicitly by soil air porosity while
13 in a more general concept soil permeability.
14
15
16
17
18
19
20

21 **1.3.1 Soil efflux relation to Reynolds Number**

22
23 The change in quantities of water, air, soil temperature, soil chemical constituents with time
24 controls the efflux intensity. That is evident from the Darcy equation [44], it is usually used
25 to model the occurring mass transport process in soil. Mainly researchers apply it for
26 calculating incompressible liquids such as for water, but it can also be applied to
27 compressible fluids such as air, carbon dioxide, etc. By applying the Darcy equation
28 specifically for carbon dioxide results in equation (1.13). This is for a specified volume of
29 soil with one of its inlets located at the bottom of the soil layer (O Horizon) and outlet is
30 located at the soil interface with the atmosphere. The parameters that govern the transport
31 properties are gas viscosity: μ_{CO_2} [Pa.s]. The soil layer depth thickness is taken as L [m], The
32 soil sample permeability k [m^2]. The sample area cross section is referred to as A [m^2]. The
33 carbon dioxide partial pressure difference is taken at two points of the O Horizon, the first at
34 the soil surface $p_{\text{SurfaceCO}_2}$ [Pa] and the second at the bottom of the soil layer p_{BottomCO_2} [Pa].
35
36 All this leads to calculate the carbon dioxide volumetric flow rate Q_{CO_2} [m^3/s], considering
37 the flow direction from inside the soil to the atmospheric interface:
38
39
40
41
42
43
44
45
46
47
48
49
50
51
52
53
54
55
56
57
58
59
60
61
62
63
64
65

$$Q_{CO_2} = -\frac{kA}{\mu_{CO_2}} \frac{(p_{SurfaceCO_2} - p_{BottomCO_2})}{L} \quad (1.13)$$

Carbon dioxide partial pressure difference can be calculated by measuring the total pressure at two points. The top soil pressure (surface) is P_{TS} [Pa], and the bottom soil pressure is P_{TB} [Pa]. Likewise molar ratios are used to represent carbon dioxide concentration at both the soil surface and at the bottom of the soil layer:

$$p_{SurfaceCO_2} - p_{BottomCO_2} = \frac{n_{SurfaceCO_2}}{n_t} P_{TS} - \frac{n_{BottomCO_2}}{n_t} P_{TB} \quad (1.14)$$

By applying equation (1.14) into (1.13) gives equation (1.15) where molar concentration on the soil surface is $[CO_2]_S$ and at the soil bottom layer is $[CO_2]_B$:

$$Q_{CO_2} = -\frac{kA}{\mu_{CO_2}} \frac{([CO_2]_S \cdot P_{TS} - [CO_2]_B \cdot P_{TB})}{L} \quad (1.15)$$

By multiplying both sides of the equation by carbon dioxide density and dividing by (cross sectional area and carbon dioxide molecular weight) the efflux equation becomes (1.16):

$$ef = -\frac{k \cdot \rho_{CO_2}}{MW_{CO_2} \cdot \mu_{CO_2}} \frac{([CO_2]_S \cdot P_{TS} - [CO_2]_B \cdot P_{TB})}{L} \quad (1.16)$$

The Darcean velocity q_{CO_2} [m/s] can be calculated from equation (1.17):

$$q_{CO_2} = -\frac{k}{\mu_{CO_2}} \nabla p_{CO_2} \quad (1.17)$$

Hence by applying the pressure derivative to equation (1.17) leads to (1.18):

$$q_{CO_2} = -\frac{k}{\mu_{CO_2}} \frac{([CO_2]_S \cdot P_{TS} - [CO_2]_B \cdot P_{TB})}{L} \quad (1.18)$$

1 The average pore velocity for carbon dioxide can be calculated using equation (1.19). This is
 2 by knowing the soil air porosity value ϕ and the Darcian velocity v_{CO_2} [m/s] in the soil:
 3

$$4 \quad v_{CO_2} = \frac{q_{CO_2}}{\phi} \quad (1.19)$$

5
 6
 7
 8
 9
 10 Substituting equation (1.18) into equation (1.19) results in equation (1.20) which shows the
 11 relationship between average flow velocity for carbon dioxide with porosity and
 12 permeability:
 13
 14
 15

$$16 \quad v_{CO_2} = -\frac{k}{\mu_{CO_2}\phi} \frac{([CO_2]_T \cdot P_{TS} - [CO_2]_0 \cdot P_{TB})}{L} \quad (1.20)$$

17
 18
 19
 20
 21
 22
 23 With occurring pressure gradients on the soil surface produced by blowing winds, suction
 24 occurs at one location and blowing occurs at another what connects both points are the soil
 25 gas cavities, this pressure difference between two points in response creates a flow in the
 26 various soil layers, for simplicity it can be very much described as underground mine
 27 ventilation principle. This is for the reason that soil structural cavities are connected in a
 28 random manner.
 29
 30
 31
 32
 33
 34
 35
 36

37
 38 For the case of microscopic fluid dynamics [45] energy transfer in the fluid is accomplished
 39 by molecular interaction (diffusion). This is where the average pore velocity q_{CO_2} and the
 40 average characteristic length scale for pores \bar{d} . The Reynolds number for soil (porous media)
 41 is given by equation (1.21):
 42
 43
 44
 45
 46
 47
 48
 49

$$50 \quad Re = \frac{\rho_{CO_2} q_{CO_2} \bar{d}}{\mu_{CO_2}} \quad (1.21)$$

51
 52
 53
 54
 55 The viscous forces dominate over the inertia forces and only the local geometry influences
 56 the flow. Knowing that the average pore velocity is in equation (1.19) then substituting it into
 57 the Reynolds number (1.21) gives:
 58
 59
 60
 61

$$Re = \frac{\rho_{CO_2} \tau v_{CO_2} \bar{d}}{\mu_{CO_2} \emptyset} \quad (1.22)$$

By substituting equation (1.21) into (1.22)

$$Re = \left| \frac{k \rho_{CO_2} \tau \bar{d} ([CO_2]_i \cdot P_{TS} - [CO_2]_0 \cdot P_{TB})}{(\mu_{CO_2} \emptyset)^2 L} \right| \quad (1.23)$$

Or by substituting equation (1.23) into (1.16) the researcher can find the relationship between the Reynolds number and the carbon dioxide efflux as shown in equation (1.24):

$$ef = Re \frac{1}{\tau \bar{d}} \frac{\mu_{CO_2} \emptyset^2}{MW_{CO_2}} \quad (1.24)$$

In porous media the flow can be characterized according to 4 regimes stated by the the author in [46]. The process is achieved by using the Reynolds number shown in equation (1.22). The power of the derived equation (1.24) can give hints to what type of flow type is occurring in the soil according to the measured efflux values. So for the first case of a Darcy or creeping flow regime it occurs when $Re < 1$. Subsequently for the second case is the inertial flow regime which occurs in ranges of $1 - 10 < Re < 150$. Meanwhile for the third case of an unsteady laminar flow regime it falls in the range of $150 < Re < 300$. Finally the fourth case is the unsteady or chaotic flow regime condition when $Re < 300$.

Considering the geometrical constraints to be fixed, external disturbances represented by the pressure term P_{TS} in equation (1.18) contributes to the transport process through the soil. Occurring blowing winds over the soil inflict changing wall shear stress over the soil creating regions of positive and negative pressure gradients, this was proved by [47] for a case of mercury vapour. An interpretation of this efflux underestimation was mentioned by [48], who stated that the effective chamber volume $V_e [m^3]$ being measured is the volume of the

1 chamber $V_c[m^3]$ including the volume of the air-filled spaces near the soil surface $V_s[m^3]$
2 where \emptyset is air porosity, this crystalizes equation in the following form (1.25):
3
4

$$5 \quad ef = \frac{V_s \emptyset + V_c}{A_s} \frac{\partial Y_{CO_2}}{\partial t} \quad (1.25)$$

6
7
8
9

10 To overcome this problem of emission underestimation, some scientists [49] have derived
11 mathematical models to study the variables that cause these underestimations. Top surface
12 soil litter dynamics dose affect soil respiration as reported by [50], forest sites have less
13 vegetation cover and more of plant dead litter [51] likewise they are characterized with high
14 water drainage rates [52] meaning that forest sites have a lower efflux in comparison with
15 grassland locations as proven by [53]. Some authors [54] have opted to measure grasslands
16 efflux at different locations between Mediterranean and Californian grassland locations. This
17 helps to see what deviations by using the proposed model would occur between the two
18 locations that unite in the same category of classification. This leads to the conclusion that
19 each site has its own characteristic efflux. This pattern becomes recognizable with
20 experiments conducted on different site locations; as a result effluxes can be fitted into site
21 categories (grassland, peatland, forest Site, rangeland, etc.).
22
23
24
25
26
27
28
29
30
31
32
33
34
35
36
37
38
39

40 It was also stated by [55] that when using a dynamic chamber, if the amount of organic
41 carbon available for microbial decomposition remains unchanged, the total amount of carbon
42 dioxide efflux will remain constant. It is known that a segment of the total flux is produced
43 by plant photosynthesis, the photosynthesis efflux depends on the density of the vegetation
44 cover in the studied location. This has lead commercial companies to make different types of
45 chambers according to the required intended flux to measure as an example: SRC-1, LI-6400,
46 SRC-MV5, CFX-2, etc. The apparatus LI-6400XT is shown on Figure 2.
47
48
49
50
51
52
53
54
55
56
57
58
59
60
61
62
63
64
65

1
2
3
4
5
6
7
8
9
10
11
12
13
14
15
16
17
18
19
20
21
22
23
24
25
26
27
28
29
30
31
32
33
34
35
36
37
38
39
40
41
42
43
44
45
46
47
48
49
50
51
52
53
54
55
56
57
58
59
60
61
62
63
64
65

Figure 2: Licor`s developed apparatus that measures photosynthesis LI-6400XT [56].

1.4 Respiration Chamber Shape, Operation Mode and Design Regulations

Many commercial companies have introduced different chamber designs, (e.g. LI-COR) as shown in Figure 3 to measure carbon dioxide fluxes and other gases of interest such as (CH₄, NO_x, etc.), these have been developed and regular functionality bugs have been resolved for the end user.

Figure 3: Available commercial chambers by Li-COR LI-8100A Automated Soil Gas Flux System [57].

An agreement in the research community is noticed on the four shape configurations of cube, cuboid, cylinder and hemisphere for small and medium sized chambers; for large applications other configurations have been surveyed by [58] such as the 8 greenhouse types shown in Figure 4. Unfortunately the majority of commercial chambers are still expensive [59]. There are four common chamber operating regimes for the ones that use gas sensors in the market today; all revolve around the following four working modes [8]: closed dynamic, closed static [60], open dynamic and open static.

Figure 4:The eight types of greenhouse configurations [58] .

The closed chamber approach is where the chamber is placed over the soil without the existence of any opening to the atmosphere from the chambers outer shell. The open chamber method is where holes exist in the chambers shell to achieve pressure equilibrium between inside and the outside atmosphere likewise the same applies to temperature and species concentration. The term static refers to a chamber that either has a switched off fan or no fan at all, while dynamic refers to the existence of a gas mixture circulation method that can be

1 an internal blowing fan or an external environmental system. The four working modes have
2 been studied and site suitability operation mode according to site properties has been found
3 [61]. Operational mode is based on steady or unsteady mode flow conditions meaning that
4
5 when no induced flow is occurring in the chamber and diffusion is dominant then it can be
6
7 regarded as a steady state case, while for a case of induced convection with blowing fans in
8
9 the chamber a turbulent flow pattern would occur in the chamber characterizing it as an
10
11 unsteady state. The proposal to use automated closed chambers has been investigated by [62]
12
13 making it an attractive option in the presence of geographical restrictions, reduced equipment
14
15 costs, accuracies at high and low efflux rates, fully automated measurements and good
16
17 suitability for long term continuous measurement projects.
18
19
20
21
22
23
24

25 Several authors have specified chamber design approaches this is seen for the dynamic
26
27 chamber case in [63] in addition to a study applied to a dynamic chamber design located on a
28
29 rangeland [64]. Conversely author [41] looks more in detail to the relationship between soil
30
31 parameters and different chamber designs and how that affects efflux measurements. One
32
33 way proposed to evaluate chamber design and its system was proposed by [41], that is done
34
35 through comparing the efflux measurement for the developed one against the efflux for the
36
37 three considered chambers models. Chambers have to satisfy minimum design requirements
38
39 to perform their role to the optimum level of acceptable measurement accuracy. Commercial
40
41 chamber design companies take into consideration [65] a set of design regulations to achieve
42
43 reliable efflux measurements, these are as follows:
44
45
46
47
48
49

- 50 • Minimize the changes in the natural microclimate within the respiration chamber [66].
- 51
- 52 • Minimize disturbances of the soil, which contains the various sources of carbon
- 53
54 dioxide from plant roots to bacteria, etc.
- 55
- 56
- 57
- 58 • Cause no change to the pressure inside the respiration chamber [67].
- 59
60
61
62
63
64
65

- Cause no build up or depletion of carbon dioxide that might cause substantial changes in the gradient of carbon dioxide concentration or cause leakage of carbon dioxide into or out of the respiration chamber.
- Measure water vapour pressure with a correction factor.

1.4.1 Chamber Dimensional Factors and Outer Shell Shape considerations

Chamber dimensional factors as mentioned by [68] have proved to be a contributing factor to concentration measurement deviations. It is stated that underestimation of efflux was related to the chamber height, volume and the soil covered area together with the increase of design parameter values. These factors have been studied extensively using numerical models by [69]. From an aerodynamic perspective [70] the reason for that is due to the creation of the circulation region behind the chamber as shown in Figure 5, the intensity of the aft region depends on the blowing wind velocity.

Some chamber designers have opted to use either the cylindrical, box or hemisphere shape; the shape selection criteria is mainly based on the ease of manufacture, and on the manufacturing funds allocated for the research project. Height of chamber as emphasized by [71] is of importance as the study investigated the effect of chamber heights ranging from 5 [cm] to 30 [cm]. The majority of chambers are about half a meter or less in height. Consequently this means that usually chambers interacts with the flow boundary layer. The respiration chamber according to its height H [m] can be determined if it is submerged in the boundary layer [72] thickness δ [m] using equation (1.27). The researcher would encounter two cases during the aerodynamic design process that is he either knows the distance where the boundary layer starts from, or he knows the thickness of the boundary layer based on assuming that it is bigger or equal to the chamber height.

1.4.2 The Cylindrical Shape Respiration Chamber

Speaking of the first case considering an external laminar flow regime occurs. The distance downstream from the start of the boundary layer is x [m] and the Reynolds number relating to the boundary layer distance is shown in equation (1.26). Where air density is ρ [kg/m³] while u_∞ [m/s] is the free stream velocity and the air dynamic viscosity is μ [Pa. s].

$$Re_x = \frac{\rho u_\infty x}{\mu} \quad (1.26)$$

The boundary layer thickness δ [m] is calculated from equation (1.27):

$$\delta \approx 4.91 \frac{x}{\sqrt{Re_x}} \quad (1.27)$$

The chamber can only be submerged if it satisfies the following condition (1.28) for the laminar flow case, where H [m] is the chamber height:

$$\delta > H \quad (1.28)$$

To calculate the boundary layer thickness for an external turbulent flow is by using equation (1.29). Note it has the same defined variables as equation (1.27):

$$\delta \approx 0.328 \frac{x}{Re_x^{1/5}} \quad (1.29)$$

Again the chamber can only be submerged if it satisfies the following condition (1.30) for a turbulent flow case:

$$\delta > H \quad (1.30)$$

1 The second case is where boundary layer thickness is assumed to be known. Whereby it is equal
2 to chamber height or over $\delta \geq H$ this is for a laminar case. Then by substituting equation
3 (1.26) into (1.27) and dealing with the parameter of distance x as an unknown equation (1.31)
4 is derived:
5
6
7
8
9

$$10 \quad x = 24.1 \frac{\rho u_{\infty} H^2}{\mu} \quad (1.31)$$

11
12
13
14
15 To avoid repetition the same approach can be applied for the turbulent boundary layer case
16 which results in equation (1.32):
17
18
19
20

$$21 \quad x = 263.4 \left(\frac{\rho u_{\infty}}{\mu} \right)^{1/4} H^{5/4} \quad (1.32)$$

22
23
24
25 In conclusion in open spaces of chamber deployment where no obstacles of different heights
26 are distributed around the chamber boundary layers would occur at some distance x around
27 the chamber. Likewise what lessens the impact of generated boundary layers on chambers is
28 by deploying it to locations that either have reasonably low wind speeds or the height of
29 plantation or obstacles is similar to the chambers height. This is sometimes referred to by
30 meteorologists as surface roughness.
31
32
33
34
35
36
37
38
39
40

41 The boundary layer occurs as the flow runs parallel to the soil surface [73] it helps in
42 dampening the occurring flow disturbance at the head of the chamber till some point.
43 Consequently it all depends on the continuity of kinetic energy provided by the blowing
44 winds to the external flow around the chamber to preserve the created boundary layer. It is
45 stated in [68] that tall chambers over estimate efflux measurements this can be attributed to
46 the generated horse shoe and arch vortex as shown in Figure 5. The trailing vortex has a
47 minor affect, because its intensity increases as it moves away from the chamber. To tackle the
48
49
50
51
52
53
54
55
56
57
58
59
60
61
62
63
64
65

1
2
3
4
5
6
7
8
9
10
11
12
13
14
15
16
17
18
19
20
21
22
23
24
25
26
27
28
29
30
31
32
33
34
35
36
37
38
39
40
41
42
43
44
45
46
47
48
49
50
51
52
53
54
55
56
57
58
59
60
61
62
63
64
65

problem of the arch and horseshoe vortex designers are advised to see how they are generated, the generation process is described in detail by [74].

Figure 5: The occurring flow pattern around a cylindrical chamber [70]. What affects mainly the measurement is the horseshoe vortex, arch vortex.

External flows refer to blowing winds occurring externally around the chamber shell. During the design process of a chamber, two important dimensionless numbers are used in the phase of occurring flow pattern characterization. These are the Reynolds (1.33) and the Strouhal numbers (1.34). The Reynolds number is calculated in relation to the dimensional characteristic length L [m] of the chamber. The average flow velocity at the studied location is \bar{U} [m/s] and ϑ [Pas] is the kinematic viscosity [m^2/s] for air. Hence L [m] can be the chamber diameter for a cylinder shape case and. The Reynolds number:

$$\text{Re} = \frac{\bar{U}L}{\vartheta} \quad (1.33)$$

The Strouhal Number (1.34) has the same two terms of dimensional characteristic length and average flow velocity used in (1.33). The vortex shedding frequency is f [s^{-1}] :

$$\text{St} = \frac{fL}{\bar{U}} \quad (1.34)$$

Lots of aerodynamic material is available for cylinders in relation to St and Re numbers, which allows the chamber designer to find the critical flow frequency that causes external flow disturbance. To discuss the argument it requires the assumption of using a 1 [m] diameter cylindrical chamber with constant physical flow properties and applying it to equation (1.25). This helps in finding the external wind blowing velocity relation to the Reynolds regime characterization.

Looking at Figure 6 the first flow regime is for the case of unseparated flow represented by the condition (1.35). This is for a calm day with no obvious blowing winds $u < 7.1 \times 10^{-5}$ [m/s], consequently no expected under or over flux measurements.

$$5 < Re \tag{1.35}$$

Cylindrical chambers usually are usually deployed on sites that are characterized to have blowing velocities in the range of 7.1×10^{-5} [m/s] $< u < 6 \times 10^{-4}$ [m/s] meaning the flow regime exists in the range of (1.36) and is described to have a fixed pair of foppl vortices in wake. Hence less accurate efflux measurements will result due to the generated weak arch vortex.

$$5 < Re < 40 \tag{1.36}$$

Figure 6: A summary of the 6 cases of external flows occurring around a cylinder represented in relation to the Reynolds number for flow characterization [75].

Small wind flow velocities in the range of 6×10^{-4} [m/s] $< u < 0.02$ [m/s] are characterised for the case of (1.37). This is where two regimes are considered, the flow starts off at $Re=40$ in which the vortex street is laminar and moves on to the transitional stage at $Re=150$. The vortex transition stage from laminar to turbulent is located between $Re=150$ and $Re=300$. The first discussed phase the vortex street is laminar meaning that the arch vortex is still weak to create a substantial negative pressure region after the chamber. The second phase is when the

1 vortex street start developing in a full turbulent vortex this is when the frequency and strength
2 of the suction affect becomes evident on the measurements by the arch vortex.
3

$$4 \quad 40 < Re < 300 \quad (1.37)$$

5
6
7
8
9 The majority of site locations have average wind flow velocities in the range of 0.02 [m/s]
10 $\langle u \rangle < 5$ [m/s] meaning they are characterized by (1.38). This is the case where Vortex Street is
11 fully turbulent.
12
13
14

$$15 \quad 300 < Re < 3.5 \times 10^5 \quad (1.38)$$

16
17 Wind blowing velocities are in the range of 5 [m/s] $\langle u \rangle < 50$ [m/s] as characterized in (1.39).
18
19
20
21
22
23
24
25
26
27
28
29
30
31
32
33
34
35
36
37
38
39
40
41
42
43
44
45
46
47
48
49
50
51
52
53
54
55
56
57
58
59
60
61
62
63
64
65

$$3.5 \times 10^5 < Re < 3.5 \times 10^6 \quad (1.39)$$

Reported cyclone wind velocities [76] are 35 [m/s] this is the maximum anticipated velocity.
Therefore the case (1.40) represents the case of reestablishment of turbulent vortex street,
hence fitting to the last stated category towards the bottom of Figure 6. This case rarely
happens and can be regarded as the maximum value case for specific chamber designs to be
deployed in the regions of cyclones.

$$3.5 \times 10^6 < Re_{\text{Cyclone}} \quad (1.40)$$

This leads to the conclusion for cylindrical chambers that by predicting the Strouhal number
for a certain external flow regime the intensity and frequency of the occurring vortex
shedding can be found using equation (1.34). Hence over or under prediction of efflux
measurements can be corrected. The relationship between the Strouhal and Reynolds number

1
2
3 for a cylinder case in the range $40 < Re < 1200$ is shown in equation (1.41) it is proposed by
4
5 [77]:

$$6 \quad St = 0.2731 - \frac{1.1129}{\sqrt{Re}} + \frac{0.4821}{Re} \quad (1.41)$$

7
8
9

10 Therefore it is recommended to have prior data of probability distribution of annual wind
11 blowing velocities on the site of interest. This is done either through the use of histograms,
12 Rayleigh or Weibull methods as shown by [78]. Consequently this helps to determine the
13 compatibility of the chamber shape with its planned location of installation.
14
15
16
17
18
19
20
21
22
23

24 **Figure 7:** Probability distribution of annual wind speeds example.

25 26 **1.4.3 The Box Shape Respiration Chamber**

27
28 Box chambers cause earlier flow separation [79] if they are positioned exactly in the face of
29 the flow, as shown in Figure 8. What mainly causes the disturbance is the horseshoe vortex
30 at the prism wall junction and on a much minor scale the base vortex structures. In conclusion
31 it is best to record the occurring wind blowing directions before setting up the chamber on
32 location. Then, the chamber can be placed in a wedge type flow configuration to lessen the
33 aft flow disturbance over the soil surface which in result affects the efflux measurements.
34
35
36
37
38
39
40
41
42
43
44
45
46
47

48 **Figure 8:** The box shaped chamber with the horseshoe vortex at prism-wall junction, this
49 vortex which mainly disturbs concentration measurements in the chamber [79].
50

51 For static chambers some researchers [80] have used small in height chambers as shown in
52 Figure 9. This kind of approach is recommended based on the principle that gas species take
53 time to diffuse therefore small in height chambers reduces data measurement time. Using
54 small sized chambers as shown by [75] can decrease the amount of disturbance but on the
55
56
57
58
59
60
61
62
63
64
65

1 other hand, it can affect the accuracy of the measured location emissions. That can be evident
2 for the case use (SRC-1, height: 150 [mm]) or (CPY-4, height: 145 [mm]) both produced by
3 PP Systmes [81]. Chamber designers have also opted to use flexible designs, for the case of
4 tall plants where two chambers are fitted in parallel.
5
6
7
8
9

10
11
12
13
14 **Figure 9:** A small in height static chamber.
15

16 **1.4.4 The Hemispherical Shape Respiration Chamber**

17
18 Some researchers have proposed the use of hemispherical shaped type chambers as found in
19 [73] and in [79]. Hemispherical chambers (dome shaped) [82] are found to be preferable
20 because they don't cause the top head vortex disturbance as seen in the cylindrical Figure 6
21 and box chamber case Figure 8. They do generate tip hairpins as illustrated by [83] but
22 usually they are drawn away by the occurring boundary layer.
23
24
25
26
27
28
29
30

31 The setback in using cylindrical shape chambers is that they produce vortex shedding behind
32 them at site locations characterized with high blowing winds. Avoiding sharp edges on the
33 chambers outer shell is also required to avoid sources of flow turbulence to the external flow.
34 It has been pointed out by [76] that external shape irregularities introduce disturbance to the
35 occurring flow around the chamber. It is noticeable in Figure 10 that chamber designers of
36 LI-8100A have filleted the occurring edges of the apparatus in addition to use the collar
37 method to lessen the side effects of apparatus shape irregularities.
38
39
40
41
42
43
44
45
46
47
48
49

50 **Figure 10:** LI 8100A Automated Soil CO₂ Flux System and soil chambers provided by
51 LICOR [84].
52
53
54
55

56 This sets the emphasises for designers that a streamlined chamber outer and inner shell is
57 recommended so that negative pressure regions don't occur on the surface of neighbouring
58
59
60
61
62
63
64
65

soil outside or inside of the chamber. The negative and positive pressure regions distributed randomly inside and around the chamber cause leakage in and out of the chamber (mass transport fluxes), more over pressure affects are covered extensively on page **Error! Bookmark not defined.** This is based on the pressure difference through soil porous media according to Darcy law equation (1.13). On the other hand classical shapes are much easier to manufacture than streamlined chamber shells. Consequently relatively small respiration chambers should be tested in wind tunnels. However large in size chambers or greenhouses can be tested using commercial CFD packages [85]. Therefore for the purpose of chamber design evaluation CFD can prove to be less costly before conducting full-size practical tests.

1.4.5 Chamber Static Stability over the Site of Installation

Designers can use equation (1.45) to approximate the chamber static stability over the site of installation while blowing wind occurs. This is by applying the equilibrium of torque at the corner edge of the chamber as shown in (1.42). For this case we apply (1.42) for a cylindrical shape chamber, the same principle can be applied for other shapes. The wind torque is T_{wind} [Nm] and the weight torque is T_{weight} [Nm] :

$$\sum_i T_n = T_{wind} - T_{weight} = 0 \quad (1.42)$$

Substituting into equation (1.42) both the acting wind force F_{wind} [N] and the chamber weight force F_w [N] results in equation (1.43). Additionally h [m] is the lever arm for the wind force, while radius R [m] is the lever arm for the chamber weight force.

$$F_{wind}h = F_w R \quad (1.43)$$

Applying into equation (1.43) the drag force equation parameters on the left hand side and Newton's second law on the right-hand side will result in equation (1.44). This is where ρ [kg/m³] is the air density, C_D is the drag force coefficient it can be obtained from

1 [86]. The flow obstructing chamber area is A_f [m^2]. Likewise on the right-hand side m [kg]
2 is the mass of the chamber furthermore the gravitational acceleration is g [m/s^2] :
3
4

$$5 \quad 0.5C_D\rho u_{cr}^2 A_f h = mgR \quad (1.44)$$

6
7
8
9 Hence the critical blowing wind velocity to achieve chamber turn over can be calculated
10 using equation (1.45):
11
12

$$13 \quad u_{cr} = \sqrt{\frac{mgR}{0.5C_D\rho A_f h}} \quad (1.45)$$

14
15
16
17
18
19
20
21 Leading to that wind velocities at the location should always be lower than the critical
22 velocity as shown in (1.46):
23
24

$$25 \quad u < u_{cr} \quad (1.46)$$

26
27
28
29 If the location has high blowing winds furthermore the condition of equation (1.46) cannot be
30 satisfied then the designer can resort to chamber fixing approaches like collars, anchoring etc.
31
32
33

34 **1.4.6 Chambers Internal Geometric Considerations.**

35
36
37
38 It is noticeable in [87] that geometrical constraints inside the chamber cause disturbance to
39 the measurements. This means the lesser the obstacles are there the better the design is, this
40 kind of approach is evident in the available research chamber [80] such as the one shown in
41
42
43
44
45
46
47
48
49
50
51
52
53
54
55
56
57
58
59
60
61
62
63
64
65

Figure 11: A chamber with no internal obstacles except the tree branches.

Therefore it is recommended to lessen the usage of the connecting beams inside the chamber
that designers usually opt to strengthen the chambers rigidity, the same applies to used wiring
or sensors inside the chamber. Cylindrical beams create vortex shedding at certain flow

1 speeds [88], sharp edges are a source of turbulence to the flow as shown for backward facing
 2 step flow [74]. This leads us to the conclusion that the existence of solid obstacles such as
 3 sharp edges, cylindrical beams, cabling or flapping paper (generates flutter) inside the
 4 chamber have a strong impact on creating flow disturbance for the case of a dynamic
 5 chamber. For a static respiration chamber case solid obstacles play a significant part in
 6 delaying the uniform diffusion of carbon dioxide in the chamber gas volume. On the other
 7 hand for the case of a static open chamber the external pressure contributes to the problem of
 8 wrong measurements [89] because external disturbance is generated by occurring blowing
 9 winds. Furthermore for the case of open dynamic chambers strong blowing winds might have
 10 disastrous effects due to the generation of pressure disturbance between the inside and
 11 outside of the chamber. Therefore the probability of the occurrence of high internal or
 12 external pressure is high. This disturbance disrupts the required pressure equilibrium
 13 condition to occur inside and outside the chamber.
 14
 15
 16
 17
 18
 19
 20
 21
 22
 23
 24
 25
 26
 27
 28
 29
 30

31 This length scale for a dynamic chamber can be considered as the blowing fan diameter
 32 length D_{Fan} [m], this is for a case where a chamber has obstacles or sharp edges which have a
 33 characteristic dimension L_S [m] smaller than the fan diameter (1.47).
 34
 35
 36
 37
 38
 39
 40
 41
 42
 43

$$D_{\text{Fan}} \geq L_S \quad (1.47)$$

44 Likewise the length scale of the turbulent flow structure depends on the characteristic length
 45 of the secondary source of turbulence, this case occurs when the fan jet hits an obstacle
 46 bigger in length than its diameter (1.48). This can be a connecting beam or some instrument
 47 inside the chamber.
 48
 49
 50
 51
 52
 53
 54
 55
 56
 57
 58
 59
 60
 61
 62
 63
 64
 65

$$D_{\text{Fan}} \leq L_S \quad (1.48)$$

1
2
3
4
5
6
7
8
9
10
11
12
13
14
15
16
17
18
19
20
21
22
23
24
25
26
27
28
29
30
31
32
33
34
35
36
37
38
39
40
41
42
43
44
45
46
47
48
49
50
51
52
53
54
55
56
57
58
59
60
61
62
63
64
65

Meanwhile for the case of static chambers the Kolmogorov length scale η [m] as shown in (1.49) is the smallest scale of disturbance and is the most dominant length scale. Additionally the average rate of dissipation per unit mass is ϵ [m^2/s^3] and the kinematic viscosity ν [m^2/s]. In a dynamic chamber case Kolmogorov length scale do occur in the chamber but at less dominant magnitude.

$$\eta = \left(\frac{\nu^3}{\epsilon} \right)^{1/4} \quad (1.49)$$

The Reynolds number for inner flows mainly relies on the main length scale dimension inside the chamber. The limits for Reynolds in chambers can be found equation (1.50), to insure that least disturbance to the inner chamber environment can be obtained at the same time for chamber inner mixture circulation to occur.

$$\text{Re} \leq \text{Re}_{\text{cr}} \quad (1.50)$$

Finding the critical Reynolds number is done by assigning several blowing speeds to the circulation fan and then measuring the inner chamber pressure in addition to plotting the concentration curve in relation to time. Plotting the concentration curves in relation to time for the different fan velocities cases comes next. This helps in comparing and optimizing the process for the mentioned cases. Consequently the most reliable concentration curve is obtained while preserving the built up inner pressure to the minimum. This approach is recommended to be applied experimentally. Another but not easy approach for optimization comes in the form of calculating the flow energy spectrum inside the chamber for different inner chamber pressures. This can be conducted easily through the use of CFD codes, experimentally it is tedious and time consuming to capture the flow fields in the chamber 3D domain. Hence if the researcher wants to pursue the route of turbulence then he is advised to read through [90]. In conclusion the Strouhal number as it was used for external flows it can

1 also be applied for internal flows as in a form of disturbance frequency characterization and
2 intensity. Hence for inner flows it can be applied mainly to the cylindrical connecting inner
3 beams or to the sharp edges in the chamber. Inner beams having a circular cross section are
4 favoured in comparison with the ones that have a box cross section, for the purpose of
5 reducing the number of sharp edges used down to two. Sharp edges and inner beams are
6 unwanted for designers in a chamber hence one way around such a geometrical constraints is
7 to use them if needed at a small scale in heights and diameters. Consequently designers can
8 rely on the viscous forces occurring in the flow as well as the Kolmogorov length scales
9 concentrated near the flow stagnation regions to dampen the flow disturbance.
10
11
12
13
14
15
16
17
18
19
20
21

22 **1.5 Conclusion**

23 Soil geomechanical and physical factors affect the measured efflux in respiration chambers
24 likewise meteorological acting disturbances on the chamber cause deviations in carbon
25 dioxide measurements. Consequently prior shape selection is of importance according to
26 location wind speed histograms. Likewise the interaction of the chambers outer shape with
27 blowing winds cannot be neglected. In conclusion different shape chambers produce different
28 flow structures meaning flow turbulence should be considered during the chamber design
29 stage. These flow structures are characterized having different strength intensities whereby
30 they cause regions of high and low pressure over the soil surface near the chamber. Hence
31 they cause over or under prediction of measured carbon dioxide fluxes. Hence preserving the
32 internal chamber environment is a necessity this can be done by using the air heat exchanger
33 system (EAHE) mentioned in [91, 92].
34
35
36
37
38
39
40
41
42
43
44
45
46
47
48
49
50
51

52 **1.6 Acknowledgments**

53 We would also like to thank all members of the Institute of Engineering and Energy
54 Technologies (IEET) and Institute of Thin Films, Sensors & Imaging at the University of
55 UWS in providing the necessary facilities to conduct such research.
56
57
58
59
60
61
62
63
64
65

1
2
3
4
5
6
7
8
9
10
11
12
13
14
15
16
17
18
19
20
21
22
23
24
25
26
27
28
29
30
31
32
33
34
35
36
37
38
39
40
41
42
43
44
45
46
47
48
49
50
51
52
53
54
55
56
57
58
59
60
61
62
63
64
65

References

1. Olabi, A., 100% sustainable energy. Energy, 2014. **77**: p. 1-5.
2. Alaswad, A., et al., Technologies and developments of third generation biofuel production. Renewable and sustainable energy reviews, 2015. **51**: p. 1446-1460.

- 1
2
3
4
5
6
7
8
9
10
11
12
13
14
15
16
17
18
19
20
21
22
23
24
25
26
27
28
29
30
31
32
33
34
35
36
37
38
39
40
41
42
43
44
45
46
47
48
49
50
51
52
53
54
55
56
57
58
59
60
61
62
63
64
65
3. Olabi, A.G., Developments in sustainable energy and environmental protection. *Energy*, 2012. **39**(1): p. 2-5.
4. Olabi, A.G., The 3rd international conference on sustainable energy and environmental protection SEEP 2009–Guest Editor’s Introduction. *Energy*, 2010. **35**(12): p. 4508-4509.
5. Ahmed Al Makky, A.A., Desmond Gibson and A.G.Olabi, Renewable Energy Scenario and Environmental Aspects of Soil Emission Measurements. Paper accepted in *Renewable and Sustainable Energy Reviews*, 2016.
6. Levine, J.S., Measurement of nitrogen oxide emissions from an agricultural soil with a dynamic chamber system. *Journal of geophysical research*, 1999. **104**(D1): p. 1609-1619.
7. Cambardella, C., et al., Field-scale variability of soil properties in central Iowa soils. *Soil Science Society of America Journal*, 1994. **58**(5): p. 1501-1511.
8. Kutsch, W.L., M. Bahn, and A. Heinemeyer, *Soil carbon dynamics: an integrated methodology* 2009: Cambridge University Press.
9. Raich, J.W. and C.S. Potter, Global patterns of carbon dioxide emissions from soils. *Global Biogeochemical Cycles*, 1995. **9**(1): p. 23-36.
10. Bazzaz, F.A., The response of natural ecosystems to the rising global CO₂ levels. *Annual review of ecology and systematics*, 1990: p. 167-196.
11. Joos, F., G. Müller-Fürstenberger, and G. Stephan, Correcting the carbon cycle representation: How important is it for the economics of climate change? *Environmental Modeling & Assessment*, 1999. **4**(2-3): p. 133-140.
12. Cramer, W., et al., Global response of terrestrial ecosystem structure and function to CO₂ and climate change: results from six dynamic global vegetation models. *Global Change Biology*, 2001. **7**(4): p. 357-373.

- 1
2
3
4
5
6
7
8
9
10
11
12
13
14
15
16
17
18
19
20
21
22
23
24
25
26
27
28
29
30
31
32
33
34
35
36
37
38
39
40
41
42
43
44
45
46
47
48
49
50
51
52
53
54
55
56
57
58
59
60
61
62
63
64
65
13. Omer, A.M., Energy, environment and sustainable development. *Renewable and sustainable energy reviews*, 2008. **12**(9): p. 2265-2300.
14. Evans, A., V. Strezov, and T.J. Evans, Assessment of sustainability indicators for renewable energy technologies. *Renewable and sustainable energy reviews*, 2009. **13**(5): p. 1082-1088.
15. Omer, A.M., Power, people and pollutions. *Renewable and sustainable energy reviews*, 2008. **12**(7): p. 1864-1889.
16. Banos, R., et al., Optimization methods applied to renewable and sustainable energy: A review. *Renewable and sustainable energy reviews*, 2011. **15**(4): p. 1753-1766.
17. Bugaje, I., Renewable energy for sustainable development in Africa: a review. *Renewable and sustainable energy reviews*, 2006. **10**(6): p. 603-612.
18. Omer, A.M., Green energies and the environment. *Renewable and sustainable energy reviews*, 2008. **12**(7): p. 1789-1821.
19. Sumathi, S., S. Chai, and A. Mohamed, Utilization of oil palm as a source of renewable energy in Malaysia. *Renewable and sustainable energy reviews*, 2008. **12**(9): p. 2404-2421.
20. Niven, R.K., Ethanol in gasoline: environmental impacts and sustainability review article. *Renewable and sustainable energy reviews*, 2005. **9**(6): p. 535-555.
21. Mata, T.M., A.A. Martins, and N.S. Caetano, Microalgae for biodiesel production and other applications: a review. *Renewable and sustainable energy reviews*, 2010. **14**(1): p. 217-232.
22. Hepbasli, A., A key review on exergetic analysis and assessment of renewable energy resources for a sustainable future. *Renewable and sustainable energy reviews*, 2008. **12**(3): p. 593-661.

23. Bhat, I. and R. Prakash, LCA of renewable energy for electricity generation systems—a review. *Renewable and sustainable energy reviews*, 2009. **13**(5): p. 1067-1073.
24. Alanne, K. and A. Saari, Distributed energy generation and sustainable development. *Renewable and sustainable energy reviews*, 2006. **10**(6): p. 539-558.
25. Jassal, R., et al., Relationship between soil CO₂ concentrations and forest-floor CO₂ effluxes. *Agricultural and Forest Meteorology*, 2005. **130**(3): p. 176-192.
26. Cussler, E.L., *Diffusion: mass transfer in fluid systems* 2009: Cambridge university press.
27. Nay, S.M., K.G. Mattson, and B.T. Bormann, Biases of chamber methods for measuring soil CO₂ efflux demonstrated with a laboratory apparatus. *Ecology*, 1994: p. 2460-2463.
28. Koorevaar, P., G. Menelik, and C. Dirksen, *Elements of soil physics*. Vol. 13. 1983: Elsevier.
29. YONEMURA, S., et al., Soil CO₂ concentrations and their implications in conventional and no-tillage agricultural fields. *農業気象*, 2009. **65**(2): p. 141-149.
30. Hanson, P., et al., Separating root and soil microbial contributions to soil respiration: a review of methods and observations. *Biogeochemistry*, 2000. **48**(1): p. 115-146.
31. Rochette, P., et al., Description of a dynamic closed chamber for measuring soil respiration and its comparison with other techniques. *Canadian journal of soil science*, 1997. **77**(2): p. 195-203.
32. Ng, B., et al., Carbon fluxes from an urban tropical grassland. *Environmental Pollution*, 2014.
33. Scurlock, J. and D. Hall, The global carbon sink: a grassland perspective. *Global Change Biology*, 1998. **4**(2): p. 229-233.

- 1
2
3
4
5
6
7
8
9
10
11
12
13
14
15
16
17
18
19
20
21
22
23
24
25
26
27
28
29
30
31
32
33
34
35
36
37
38
39
40
41
42
43
44
45
46
47
48
49
50
51
52
53
54
55
56
57
58
59
60
61
62
63
64
65
34. Najafpour, G., *Biochemical engineering and biotechnology* 2006: Elsevier.
 35. Dilly, O., Microbial respiratory quotient during basal metabolism and after glucose amendment in soils and litter. *Soil Biology and Biochemistry*, 2001. **33**(1): p. 117-127.
 36. Smith, K., et al., Exchange of greenhouse gases between soil and atmosphere: interactions of soil physical factors and biological processes. *European Journal of Soil Science*, 2003. **54**(4): p. 779-791.
 37. Smith, K., Exchange of greenhouse gases between soil and atmosphere: interactions of soil physical factors and biological processes. *Advances in Animal Biosciences*, 2010. **1**(01): p. 360-360.
 38. Pengthamkeerati, P., et al., Soil carbon dioxide efflux from a claypan soil affected by surface compaction and applications of poultry litter. *Agriculture, ecosystems & environment*, 2005. **109**(1): p. 75-86.
 39. Conklin, A.R., *Introduction to soil chemistry: Analysis and instrumentation* 2013: John Wiley & Sons.
 40. Sanci, R., H.O. Panarello, and H.A. Osters, Assessment of soil moisture influence on CO₂ flux: a laboratory experiment. *Environmental geology*, 2009. **58**(3): p. 491-497.
 41. Butnor, J.R., K.H. Johnsen, and C.A. Maier, Soil properties differently influence estimates of soil CO₂ efflux from three chamber-based measurement systems. *Biogeochemistry*, 2005. **73**(1): p. 283-301.
 42. Marshall, T., A relation between permeability and size distribution of pores. *Journal of Soil Science*, 1958. **9**(1): p. 1-8.
 43. McNeill, A. and P. Kolesik, X-ray CT investigations of intact soil cores with and without living crop roots. *Super Soil*, 2004.
 44. Barnes, G.E., *Soil mechanics: principles and practice* 2010: Palgrave macmillan.

- 1
2
3
4
5
6
7
8
9
10
11
12
13
14
15
16
17
18
19
20
21
22
23
24
25
26
27
28
29
30
31
32
33
34
35
36
37
38
39
40
41
42
43
44
45
46
47
48
49
50
51
52
53
54
55
56
57
58
59
60
61
62
63
64
65
45. Kaviany, M., Principles of heat transfer in porous media 1995: Springer.
 46. Kaviany, M., Principles of heat transfer in porous media 2012: Springer Science & Business Media.
 47. Lin, C.-J., et al., Novel dynamic flux chamber for measuring air–surface exchange of H₂O from soils. Environmental science & technology, 2012. **46**(16): p. 8910-8920.
 48. Butnor, J.R. and K.H. Johnsen, Calibrating soil respiration measures with a dynamic flux apparatus using artificial soil media of varying porosity. European Journal of Soil Science, 2004. **55**(4): p. 639-647.
 49. Venterea, R.T., Simplified method for quantifying theoretical underestimation of chamber-based trace gas fluxes. Journal of environmental quality, 2010. **39**(1): p. 126-135.
 50. Valentini, C.M.A., et al., Soil respiration and aboveground litter dynamics of a tropical transitional forest in northwest Mato Grosso, Brazil. Journal of Geophysical Research: Biogeosciences (2005–2012), 2008. **113**(G1).
 51. Jassal, R., et al., Relationship between soil CO₂ concentrations and forest-floor CO₂ effluxes. Agricultural and Forest Meteorology, 2005. **130**(3): p. 176-192.
 52. Liang, N., et al., In situ comparison of four approaches to estimating soil CO₂ efflux in a northern larch (*Larix kaempferi* Sarg.) forest. Agricultural and Forest Meteorology, 2004. **123**(1): p. 97-117.
 53. Smith, D.L. and L. Johnson, Vegetation-mediated changes in microclimate reduce soil respiration as woodlands expand into grasslands. Ecology, 2004. **85**(12): p. 3348-3361.
 54. Xu, L. and D.D. Baldocchi, Seasonal variation in carbon dioxide exchange over a Mediterranean annual grassland in California. Agricultural and Forest Meteorology, 2004. **123**(1): p. 79-96.

- 1
2
3
4
5
6
7
8
9
10
11
12
13
14
15
16
17
18
19
20
21
22
23
24
25
26
27
28
29
30
31
32
33
34
35
36
37
38
39
40
41
42
43
44
45
46
47
48
49
50
51
52
53
54
55
56
57
58
59
60
61
62
63
64
65
55. Subke, J.A., M. Reichstein, and J.D. Tenhunen, Explaining temporal variation in soil CO₂ efflux in a mature spruce forest in Southern Germany. *Soil Biology and Biochemistry*, 2003. **35**(11): p. 1467-1483.
 56. LI-6400XT Portable Photosynthesis System. 27/08/2015]; Available from: <http://www.licor.com/env/products/photosynthesis/>.
 57. LI-8100A Automated Soil Gas Flux System. 21/08/2015]; Available from: http://www.licor.com/env/products/soil_flux/.
 58. Hobby Greenhouse Construction. 21/08/2015]; Available from: <http://www.aces.edu/pubs/docs/A/ANR-1105/index2.tmpl>.
 59. Heinemeyer, A. and N.P. McNamara, Comparing the closed static versus the closed dynamic chamber flux methodology: Implications for soil respiration studies. *Plant and soil*, 2011. **346**(1-2): p. 145-151.
 60. Pihlatie, M.K., et al., Comparison of static chambers to measure CH₄ emissions from soils. *Agricultural and Forest Meteorology*, 2013. **171**: p. 124-136.
 61. Bekku, Y., et al., Examination of four methods for measuring soil respiration. *Applied Soil Ecology*, 1997. **5**(3): p. 247-254.
 62. Delle Vedove, G., et al., Automated monitoring of soil respiration: an improved automatic chamber system. *Italian Journal of Agronomy*, 2010. **2**(4): p. 377-382.
 63. Gao, F., et al., Design, fabrication, and application of a dynamic chamber for measuring gas emissions from soil. *Environmental science & technology*, 1996. **31**(1): p. 148-153.
 64. Angell, R. and T. Svejcar, A chamber design for measuring net CO₂ exchange on rangeland. *Journal of Range Management*, 1999: p. 27-31.
 65. Luo, Y. and X. Zhou, *Soil respiration and the environment* 2006: Academic press.

- 1
2
3
4
5
6
7
8
9
10
11
12
13
14
15
16
17
18
19
20
21
22
23
24
25
26
27
28
29
30
31
32
33
34
35
36
37
38
39
40
41
42
43
44
45
46
47
48
49
50
51
52
53
54
55
56
57
58
59
60
61
62
63
64
65
66. Imhof, R., et al., Closed-chamber transepidermal water loss measurement: microclimate, calibration and performance. *International journal of cosmetic science*, 2009. **31**(2): p. 97-118.
 67. Davidson, E., et al., Minimizing artifacts and biases in chamber-based measurements of soil respiration. *Agricultural and Forest Meteorology*, 2002. **113**(1): p. 21-37.
 68. Pihlatie, M.K., et al., Comparison of static chambers to measure CH₄ emissions from soils. *Agricultural and Forest Meteorology*, 2013. **171**: p. 124-136.
 69. Gao, F. and S.R. Yates, Simulation of enclosure-based methods for measuring gas emissions from soil to the atmosphere. *Journal of Geophysical Research: Atmospheres* (1984–2012), 1998. **103**(D20): p. 26127-26136.
 70. Palau-Salvador, G., et al., Large eddy simulations and experiments of flow around finite-height cylinders. *Flow, turbulence and combustion*, 2010. **84**(2): p. 239-275.
 71. Matthias, A.D., D.N. Yarger, and R.S. Weinbeck, A numerical evaluation of chamber methods for determining gas fluxes. *Geophysical Research Letters*, 1978. **5**(9): p. 765-768.
 72. Schlichting, H. and K. Gersten, *Boundary-layer theory* 2000: Springer Science & Business Media.
 73. Fröhlich, J. and W. Rodi, LES of the flow around a circular cylinder of finite height. *International journal of heat and fluid flow*, 2004. **25**(3): p. 537-548.
 74. Simpson, R.L., Turbulent boundary-layer separation. *Annual Review of Fluid Mechanics*, 1989. **21**(1): p. 205-232.
 75. Blevins, R.D., *Flow-induced vibration*. 1990.
 76. Sparks, P. and Z. Huang, Gust factors and surface-to-gradient wind-speed ratios in tropical cyclones. *Journal of Wind Engineering and Industrial Aerodynamics*, 2001. **89**(11): p. 1047-1058.

- 1
2
3
4
5
6
7
8
9
10
11
12
13
14
15
16
17
18
19
20
21
22
23
24
25
26
27
28
29
30
31
32
33
34
35
36
37
38
39
40
41
42
43
44
45
46
47
48
49
50
51
52
53
54
55
56
57
58
59
60
61
62
63
64
65
77. Williamson, C. and G. Brown, A series in $1/\sqrt{\text{Re}}$ to represent the Strouhal–Reynolds number relationship of the cylinder wake. *Journal of Fluids and Structures*, 1998. **12**(8): p. 1073-1085.
 78. Fyrippis, I., P.J. Axaopoulos, and G. Panayiotou, Wind energy potential assessment in Naxos Island, Greece. *Applied Energy*, 2010. **87**(2): p. 577-586.
 79. McClean, J. and D. Sumner, An experimental investigation of aspect ratio and incidence angle effects for the flow around surface-mounted finite-height square prisms. *Journal of Fluids Engineering*, 2014. **136**(8): p. 081206.
 80. Kolari, P., et al., Evaluation of accuracy in measurements of VOC emissions with dynamic chamber system. *Atmospheric Environment*, 2012. **62**: p. 344-351.
 81. Systems, P. SRC-1 Soil efflux Respiration Chamber 2015; Available from: <http://ppsystems.com/soil-and-canopy-flux/>.
 82. Lin, C.-J., et al., Empirical models for estimating mercury flux from soils. *Environmental science & technology*, 2010. **44**(22): p. 8522-8528.
 83. Acarlar, M. and C. Smith, A study of hairpin vortices in a laminar boundary layer. Part 1. Hairpin vortices generated by a hemisphere protuberance. *Journal of Fluid Mechanics*, 1987. **175**: p. 1-41.
 84. Website, L.C. Automated Soil CO₂ Flux System and soil chambers. 2015 09/16/2015]; Available from: <http://www.licor.com/corp/history.html>.
 85. Ahmed Al Makky, A.G.O., A.Alaswad, D.Gibbson and S.Song, A numerical and experimental study of a new design of closed dyanmic resperiation chambers. *SEEP* 2015.
 86. White, F., *Fluid mechanics* 2015: McGraw-Hill Higher Education.

- 1
2
3
4
5
6
7
8
9
10
11
12
13
14
15
16
17
18
19
20
21
22
23
24
25
26
27
28
29
30
31
32
33
34
35
36
37
38
39
40
41
42
43
44
45
46
47
48
49
50
51
52
53
54
55
56
57
58
59
60
61
62
63
64
65
87. Pape, L., et al., An automated dynamic chamber system for surface exchange measurement of non-reactive and reactive trace gases of grassland ecosystems. *Biogeosciences*, 2009. **6**(3): p. 405-429.
 88. Szepessy, S. and P. Bearman, Aspect ratio and end plate effects on vortex shedding from a circular cylinder. *Journal of Fluid Mechanics*, 1992. **234**: p. 191-217.
 89. Xu, L., et al., On maintaining pressure equilibrium between a soil CO₂ flux chamber and the ambient air. *Journal of Geophysical Research: Atmospheres* (1984–2012), 2006. **111**(D8).
 90. Pope, S.B., *Turbulent flows2000*: Cambridge university press.
 91. Ozgener, O., L. Ozgener, and J.W. Tester, A practical approach to predict soil temperature variations for geothermal (ground) heat exchangers applications. *International Journal of Heat and Mass Transfer*, 2013. **62**: p. 473-480.
 92. Ozgener, O., L. Ozgener, and D.Y. Goswami, Experimental prediction of total thermal resistance of a closed loop EAHE for greenhouse cooling system. *International Communications in Heat and Mass Transfer*, 2011. **38**(6): p. 711-716.

List of figures:

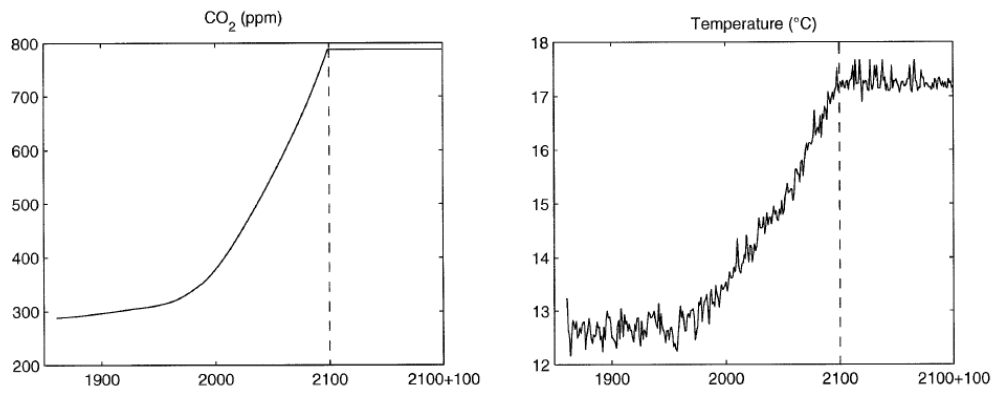


Figure 1: IPCC IS92a projections of atmospheric CO₂ concentration and the HadCM2 SUL climate model simulations of temperature over land (excluding Antarctica).



Figure 2: Licor`s developed apparatus that measures photosynthesis LI-6400XT [51].



Figure 3: Available commercial chambers by Li-COR LI-8100A Automated

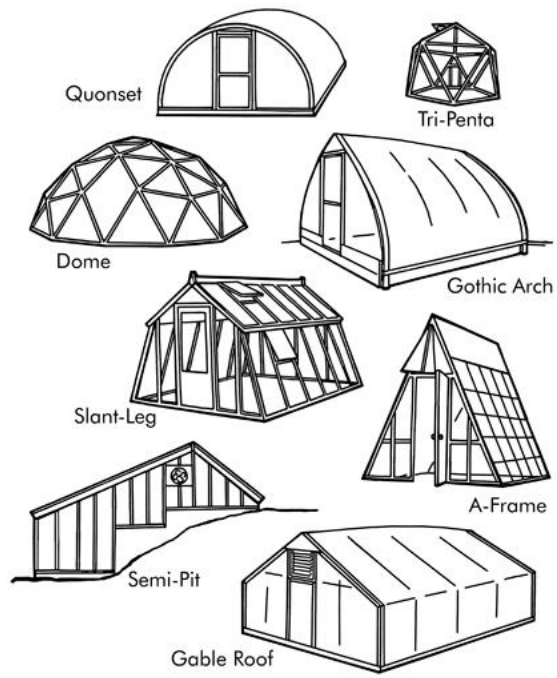


Figure 4:The eight types of greenhouse configurations [53] .

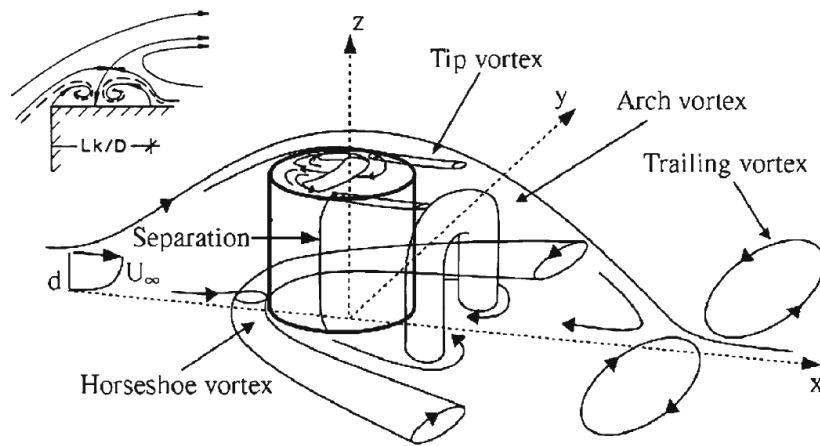


Figure 5: The occurring flow pattern around a cylindrical chamber [65]. What affects mainly the measurement is the horseshoe vortex, arch vortex.

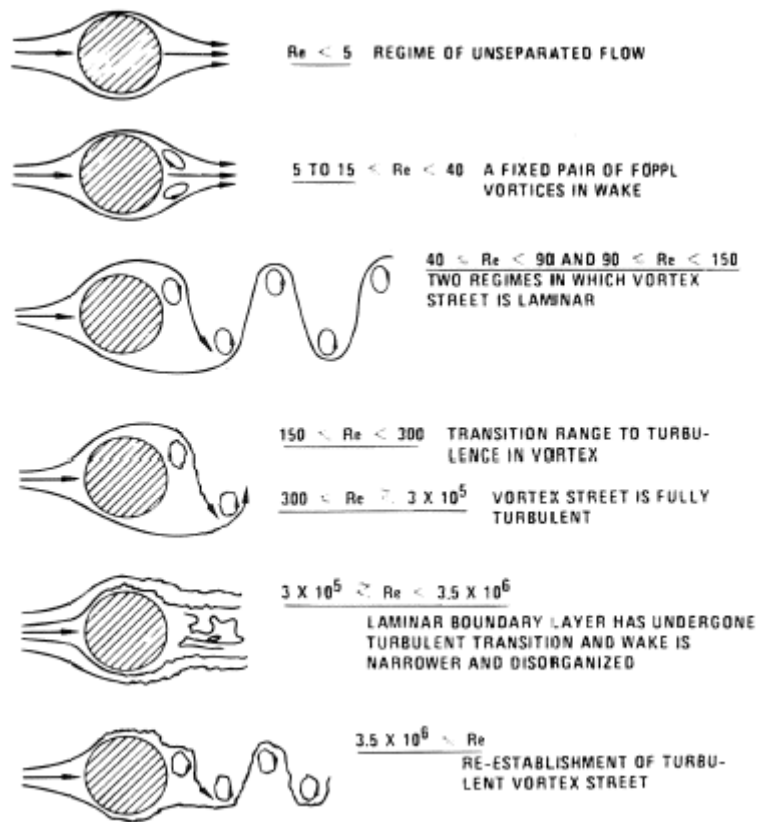


Figure 6: A summary of the 6 cases of external flows occurring around a cylinder represented in relation to the Reynolds number for flow characterization [70].

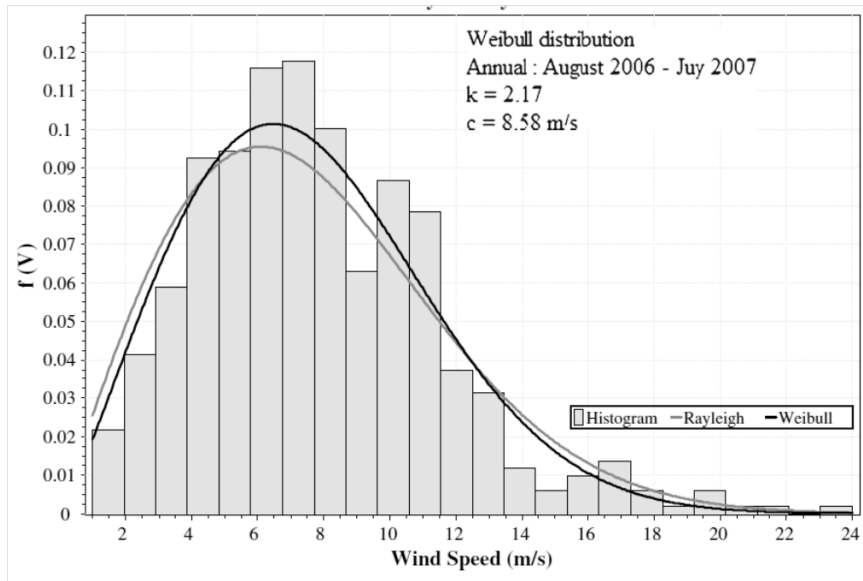


Figure 7: Probability distribution of annual wind speeds example.

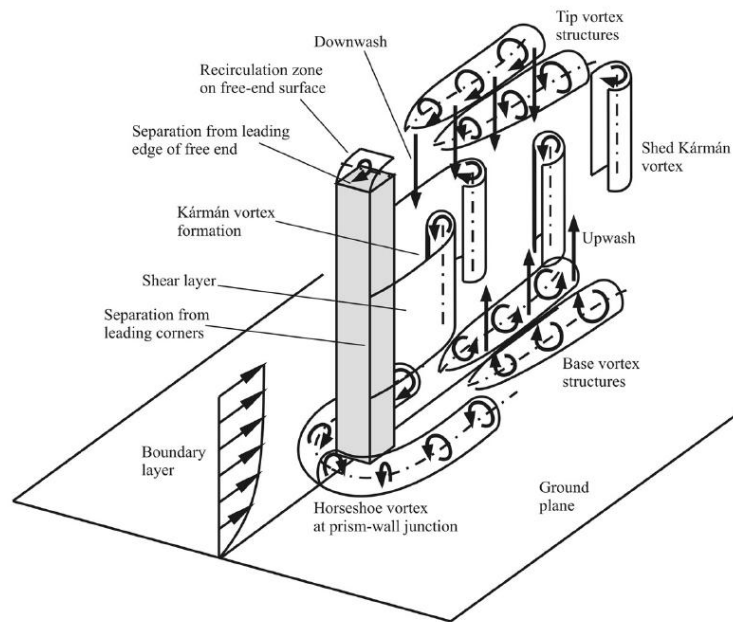


Figure 8: The box shaped chamber with the horseshoe vortex at prism-wall junction, this vortex which mainly disturbs concentration measurements in the chamber [74].



Figure 9: A small in height static chamber.



Figure 10: LI-8100A Automated Soil CO₂ Flux System and soil chambers provided by LICOR [79] .



Figure 11: A chamber with no internal obstacles except the tree branches.